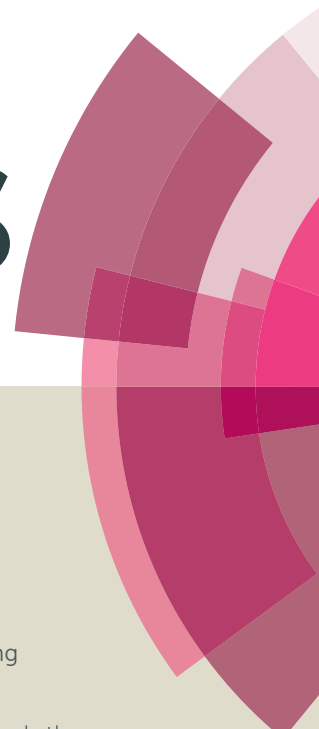


# RSC Advances



This article can be cited before page numbers have been issued, to do this please use: Y. wang, H. Song and X. Sun, *RSC Adv.*, 2016, DOI: 10.1039/C6RA21054F.



This is an *Accepted Manuscript*, which has been through the Royal Society of Chemistry peer review process and has been accepted for publication.

*Accepted Manuscripts* are published online shortly after acceptance, before technical editing, formatting and proof reading. Using this free service, authors can make their results available to the community, in citable form, before we publish the edited article. This *Accepted Manuscript* will be replaced by the edited, formatted and paginated article as soon as this is available.

You can find more information about *Accepted Manuscripts* in the [Information for Authors](#).

Please note that technical editing may introduce minor changes to the text and/or graphics, which may alter content. The journal's standard [Terms & Conditions](#) and the [Ethical guidelines](#) still apply. In no event shall the Royal Society of Chemistry be held responsible for any errors or omissions in this *Accepted Manuscript* or any consequences arising from the use of any information it contains.



## RSC Advances

## ARTICLE

Friedel-Crafts alkylation of toluene with *tert*-butyl alcohol over Fe<sub>2</sub>O<sub>3</sub>-modified H $\beta$ Yuan Yuan Wang<sup>a</sup>, Hua Song<sup>a,b,\*</sup>, Xinglong Sun<sup>c</sup>

Received 00th August 2016,

Accepted 00th August 2016

DOI: 10.1039/x0xx00000x

www.rsc.org/

Fe<sub>2</sub>O<sub>3</sub>(x)/H $\beta$  catalysts with different Fe<sub>2</sub>O<sub>3</sub> loading (x) were successfully prepared and characterized by XRD, SEM, TEM, ICP, BET, NH<sub>3</sub>-TPD and Py-IR. With selective alkylation of toluene with *tert*-butyl alcohol to produce 4-*tert*-butyltoluene as probe reaction, the effects of the different Fe<sub>2</sub>O<sub>3</sub> loading on channel structures, acidity and catalytic performance over H $\beta$  were studied. The results showed that modification of H $\beta$  with Fe<sub>2</sub>O<sub>3</sub> could adjust pore structures and decrease the total acidity, especially the strong acidity of H $\beta$ . The parent H $\beta$  exhibited the highest toluene conversion of 58.4% with the lowest PTBT selectivity of 67.3%. The low *para*-selectivity over parent H $\beta$  could be attributed to low shape-selective action of 12-ring portals of H $\beta$  and isomerization of the formed PTBT to MTBT. Upon loading of Fe<sub>2</sub>O<sub>3</sub>, the toluene conversion of Fe<sub>2</sub>O<sub>3</sub>(x)/H $\beta$  catalysts decreased slightly, but the PTBT selectivity increased significantly. The toluene conversion of 54.7% with PTBT selectivity of 81.5% were observed over Fe<sub>2</sub>O<sub>3</sub>(20%)/H $\beta$  at 190 °C after 4 h. The narrowed pores after loading the Fe<sub>2</sub>O<sub>3</sub> were benefit to increase selectivity to PTBT, since PTBT with lower kinetic diameter (0.58 nm) can diffuse through the narrowed pores of Fe<sub>2</sub>O<sub>3</sub>(x)/H $\beta$  more easily than MTBT (0.65 nm). In addition, the decrease of strong sites and deactivation of acid sites on surface are benefit to increase selectivity to PTBT by suppressing further isomerization of the formed PTBT on acid sites.

## Introduction

Acid catalyzed reactions such as Friedel-Crafts alkylation is an important process in organic synthesis, fine chemical production as well as in petrochemical process<sup>1-3</sup>. The butylated products of toluene, particularly the 4-*tert*-butyltoluene (PTBT) has great commercial significance as its derivatives 4-*tert*-butylbenzaldehyde and 4-*tert*-butylbenzoic acid are widely used in the industry<sup>4-6</sup>. Conventionally, toluene butylation reactions are carried out with alkylating agents via AlCl<sub>3</sub>, sulfuric acid and phosphoric acid as catalysts. However, these acid catalysts are not environmentally benign, not re-usable and also lead to corrosion of equipments. Therefore, considerable attention has been devoted to development of solid acid catalysts which are environmentally friendly.

It is well known that toluene is not active enough in the Friedel-Crafts alkylation in the absence of a catalyst. So, selection of a suitable catalyst is crucial to highly efficient alkylation of toluene with *tert*-butyl alcohol (TBA). Zeolites are regarded as a good choice due to their pore structures and unique acid properties. Among different zeolites, zeolite  $\beta$  with a three-dimensional (3D) interconnecting pore system and high acidity shows a high catalytic

activity. For example, Pai *et al.*<sup>7</sup> found H $\beta$  (25) and HY (30) had better catalytic activity than HMCM-22 (52) in vapour phase butylation of toluene. Mravec *et al.*<sup>8</sup> found the most active zeolite catalysts for the liquid-phase butylation of toluene were H $\beta$  (12.5) and HM (17.5). In our previous report<sup>9</sup>, we also found H $\beta$  (25) showed high catalytic activity in alkylation of toluene with TBA. However, the *para*-selectivity (4-*tert*-butyltoluene, PTBT) of 69.5% and the *meta*-selectivity (3-*tert*-butyltoluene, MTBT) of 26.9% over H $\beta$  were observed at 180 °C after 4h. It showed that the selectivity to desired product PTBT over H $\beta$  zeolite was low.

A petrochemical process is evaluated not only the basis of conversion of a given reactant, but also in terms of selectivity to desired product. Since the dimensions of 12-ring portals of parent H $\beta$  are 0.67 nm  $\times$  0.66 nm<sup>10</sup>, while the kinetic diameters are 0.58nm for PTBT and 0.65nm for MTBT<sup>8</sup>, respectively. The shape-selective action has less effect on the product selectivity to PTBT over H $\beta$  zeolite. However, the shape-selective action could be greatly improved if the 12-ring portals of parent H $\beta$  were narrowed slightly. Zeolite H $\beta$  contains numerous lattice defects due to subtle structural disorder, which is believed to create additional acid sites on internal surfaces as well as extra cation exchange positions<sup>11</sup>. Modification by metallic oxide is a highly efficient method for improving the *para*-selectivity by reducing the external acid sites and adjusting pore entrance.

As far as we know, the use of Fe<sub>2</sub>O<sub>3</sub> modification of H $\beta$  zeolites as catalysts in *tert*-butylation of toluene has not been reported. The aim of the present study was to evaluate the catalytic behaviour of Fe<sub>2</sub>O<sub>3</sub> supported on H $\beta$  for the alkylation of toluene by TBA under liquid reaction conditions. For this purpose, Fe<sub>2</sub>O<sub>3</sub>(x)/H $\beta$  samples

<sup>a</sup> College of Chemistry & Chemical Engineering, Northeast Petroleum University, Daqing 163318, Heilongjiang, China.

<sup>b</sup> Provincial Key Laboratory of Oil & Gas Chemical Technology, College of Chemistry & Chemical Engineering, Northeast Petroleum University, 163318 Daqing, China.

<sup>c</sup> Daqing Petrochemical Engineering Co., Ltd., Daqing 163714, Heilongjiang, China;

## ARTICLE

## Journal Name

containing 8–25%  $\text{Fe}_2\text{O}_3$  were prepared and were fully characterized by XRD, SEM, TEM, FT-IR, BET, TPD and Py-IR. Our objective was to correlate the channel structures and acidity of the H $\beta$  supported  $\text{Fe}_2\text{O}_3$  catalysts with their catalytic properties in alkylation of toluene.

## Experimental

### Materials

Na $\beta$  zeolite powder (Si/Al=25) was purchased from Zeolyst Int., China. Ammonium nitrate, ferric nitrate, toluene, *tert*-butyl alcohol and cyclohexane (all analytical grade) were bought from ACROS Organics and used without further purification.

### Catalyst preparation

The H $\beta$  zeolite with Si/Al ratio of 25 used in this work was prepared according to the reported procedure<sup>12</sup>. Na $\beta$  zeolite was used as a starting material. The H $\beta$  zeolite was prepared by ion exchange of Na $\beta$  with  $\text{NH}_4\text{NO}_3$  aqueous solution. After ion exchange, the zeolite was filtered, and dried at 110 °C for 12 h. Then, the samples were calcined at 550 °C for 4 h in an air atmosphere.  $\text{Fe}_2\text{O}_3$ -modified H $\beta$  zeolites support with the mass fraction of  $\text{Fe}_2\text{O}_3$  (4%, 8%, 16%, 20% and 25%) were synthesized by ion exchange of H $\beta$  zeolites with  $\text{Fe}(\text{NO}_3)_3$  aqueous solutions for 24 h at room temperature<sup>13</sup>. The resulting materials were calcined at 350 °C for 4 h in an air atmosphere. The obtained  $\text{Fe}_2\text{O}_3$ -modified H $\beta$  zeolites were denoted as  $\text{Fe}_2\text{O}_3(x)/\text{H}\beta$ , where  $x$  stood for the mass fraction of  $\text{Fe}_2\text{O}_3$  in %.

### Catalyst characterization

XRD analysis of material powders were carried out on a D/max-2200PC-X-ray diffractometer using Cu  $K\alpha$  radiation under the setting conditions of 40 kV, 30 mA, scan range from 10 to 80 at a rate of 4 °/min.

The surface morphological details of catalysts were studied by scanning electron microscopy (SEM, Zeiss-SIGMA).

The tungsten and magnesium contents of all catalysts were determined by inductively coupled plasma–optical emission spectrometry (ICP–OES) using a PerkinElmer Optima 2000DV instrument.

Nitrogen adsorption–desorption were recorded at –196 °C using Micromeritics adsorption equipment of NOVA2000e. Prior  $\text{N}_2$  adsorption, the powder samples were degassed under secondary vacuum for 1 h at 90 °C and 10 h at 180 °C. The specific surface area of each solid ( $S_{\text{BET}}$  in  $\text{m}^2/\text{g}$ ) was calculated from the adsorption isotherms using the BET method. The total pore volume ( $V_{\text{tot}}$ ) was calculated from the adsorbed volume of nitrogen at  $P/P_0$  equal to 0.99.

Samples acidity were measured by  $\text{NH}_3$  temperature-programmed desorption ( $\text{NH}_3$ -TPD) using a Quantachrome Chembet-3000 Characterization System. A 200 mg sample was pre-treated at 550 °C for 1 h in dry helium (50 mL/min) and cooled to 120 °C. It was then exposed to 10 v%  $\text{NH}_3/\text{He}$  for 1 h. After purging the catalyst with He for 1 h, a TPD plot was obtained at a heating rate of 10 °C/min from 120 to 600 °C.

IR spectra with pyridine adsorption of samples were recorded using a Bruker FT-IR spectrometer (Tensor 27) together with a high

temperature vacuum cell. The sample powder was pressed into a self-supporting wafer, and the spectra were recorded in a wavenumber range of 4000–400  $\text{cm}^{-1}$  with a 4  $\text{cm}^{-1}$  resolution. Before each experiment, material samples were pressed into thin pellets (10–30 mg) with diameter of 16 mm and activated in situ during one night under vacuum ( $10^{-5}$  Pa) at 170 °C. Pyridine was introduced in excess at 150 °C after the activation period. The concentrations of the B sites and L sites were determined from the integrated area bands of the  $\text{PyH}^+$  (located at around 1540  $\text{cm}^{-1}$ ) and  $\text{PyL}$  (around 1450  $\text{cm}^{-1}$ ) species using the values of the molar extinction coefficients of both bands.

### Toluene alkylation with *tert*-butyl alcohol

The side-chain alkylation of toluene with TBA was carried out in a laboratory autoclave reactor (300 ml) at 190 °C. At typical experiment, 10 ml of toluene (94 mmol, Aladdin, 98%) and 28 ml of *tert*-butyl alcohol (283 mmol Aladdin, 98%) were mixed with 60 ml of cyclohexane (Aladdin, 99%) solvent. Then 1.0 g of zeolite catalyst (1.35%) was added. The reaction system was sealed and purged with continuous  $\text{N}_2$  purging for 30 min. Then the mixture was heated to a certain temperature to start alkylation reaction. After reaction, the mixture was cooled down to room temperature, and the zeolite catalyst was removed by filtration. The liquid phase was analyzed on GC-14C gas chromatograph equipped with SE-30 capillary column ( $\phi$  0.25 mm  $\times$  50 m). The measurement was performed at the initial temperature of 60 °C for 2min, the ramping rate of 10 °C /min, the final temperature of 220 °C for 10 min, with nitrogen as carrier gas. During the course of the investigation, a number of runs were repeated to check for reproducibility in the experiment results, which were found to be excellent. Typical errors were in the range of  $\pm$  2%.

## Results and discussion

### Physicochemical characterization

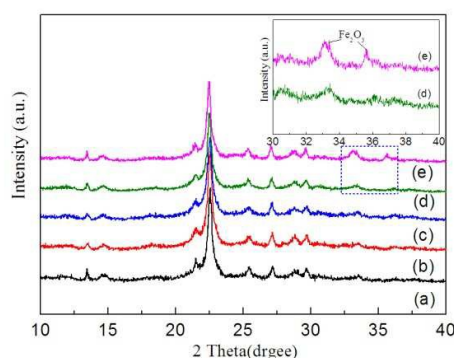


Fig 1. XRD of parent H $\beta$  and  $\text{Fe}_2\text{O}_3(x)/\text{H}\beta$

(a) parent H $\beta$ , (b)  $\text{Fe}_2\text{O}_3(8\%)/\text{H}\beta$ , (c)  $\text{Fe}_2\text{O}_3(16\%)/\text{H}\beta$ , (d)  $\text{Fe}_2\text{O}_3(20\%)/\text{H}\beta$  and (e)  $\text{Fe}_2\text{O}_3(25\%)/\text{H}\beta$

Fig.1 showed typical XRD patterns of parent H $\beta$  and  $\text{Fe}_2\text{O}_3(x)/\text{H}\beta$ . The peak positions of H $\beta$  were not changed even at high  $\text{Fe}_2\text{O}_3$  content. These results showed that the structure of H $\beta$  was retained after  $\text{Fe}_2\text{O}_3$  modification. The peaks of  $\text{Fe}_2\text{O}_3$  were not observed at  $\text{Fe}_2\text{O}_3$  contents less than 20%. This result indicated that

the  $\text{Fe}_2\text{O}_3$  was highly dispersed. Nevertheless, the peaks corresponding to  $\text{Fe}_2\text{O}_3$  appeared at  $2\theta$  of  $33.1^\circ$  and  $35.6^\circ$ <sup>14-16</sup> when the  $\text{Fe}_2\text{O}_3$  contents up to 25%. In addition, the crystallite size of  $\text{Fe}_2\text{O}_3(20\%)/\text{H}\beta$ , which was calculated using the Debye–Sherrer equation applied to the reflection at  $2\theta$  of  $22.5^\circ$ , was estimated to be 249 nm<sup>17</sup>.

Fig. 2 (a) showed the scanning electron micrograph of fresh  $\text{Fe}_2\text{O}_3(20\%)/\text{H}\beta$  sample. The crystal of fresh  $\text{Fe}_2\text{O}_3(20\%)/\text{H}\beta$  showed typical agglomerates of small cubic particles with sizes around 200–300 nm, which was in good agreement with the calculated crystallite size of  $\text{Fe}_2\text{O}_3(20\%)/\text{H}\beta$  from XRD analysis. Fig. 2 (b) showed the scanning electron micrograph of spent  $\text{Fe}_2\text{O}_3(20\%)/\text{H}\beta$  sample. There were some carbonaceous deposits on the surface of the spent  $\text{Fe}_2\text{O}_3(20\%)/\text{H}\beta$  zeolite as compared with the fresh one.

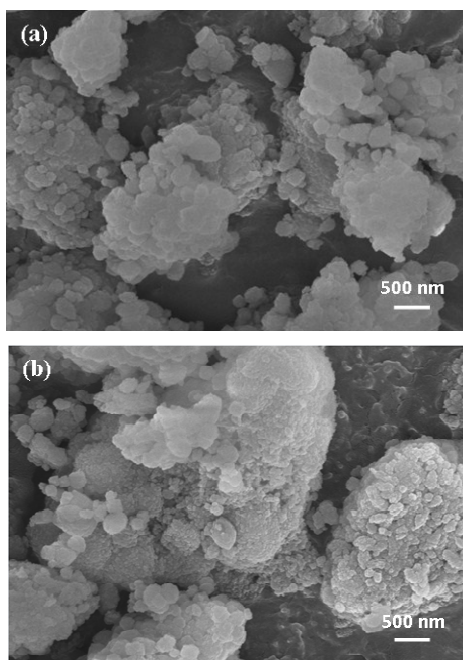


Fig. 2. SEM images obtained  $\text{Fe}_2\text{O}_3(20\%)/\text{H}\beta$   
(a) fresh  $\text{Fe}_2\text{O}_3(20\%)/\text{H}\beta$ ; (b) spent  $\text{Fe}_2\text{O}_3(20\%)/\text{H}\beta$

The transmission electron microscope of  $\text{Fe}_2\text{O}_3(20\%)/\text{H}\beta$  catalyst was shown in Fig. 3.  $\text{Fe}_2\text{O}_3(20\%)/\text{H}\beta$  showed a honeycomb structure. The  $\text{Fe}_2\text{O}_3$  was highly dispersed on  $\text{H}\beta$ , which could be distinguished as dark dots in TEM images.

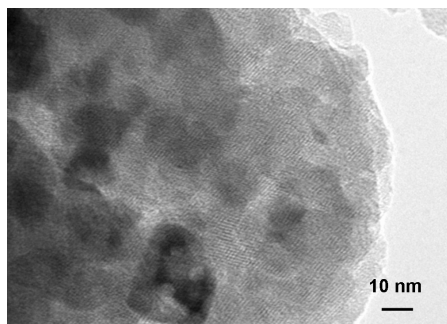


Fig. 3. TEM images obtained  $\text{Fe}_2\text{O}_3(20\%)/\text{H}\beta$

As can be seen from Table 1, the actual loading amounts of  $\text{Fe}_2\text{O}_3$  in the fresh  $\text{Fe}_2\text{O}_3(x)/\text{H}\beta$  materials obtained from ICP measurement were close to their corresponding theoretical amounts. However, the amount of  $\text{Fe}_2\text{O}_3$  in spent  $\text{Fe}_2\text{O}_3(20\%)/\text{H}\beta$  was 19.5%, which was slightly lower than that found in the fresh one (19.8%). The leaching of  $\text{Fe}_2\text{O}_3$  into the reaction mixture was responsible to the low amount of  $\text{Fe}_2\text{O}_3$  in the spent  $\text{Fe}_2\text{O}_3(20\%)/\text{H}\beta$ .

Table 1 The structural parameters of parent  $\text{H}\beta$  zeolite and  $\text{Fe}_2\text{O}_3(x)/\text{H}\beta$  zeolites

Zeolites	Content of $\text{Fe}_2\text{O}_3^a$ (%)	BET surface area <sup>b</sup> ( $\text{m}^2/\text{g}$ )	Pore volume <sup>c</sup> ( $\text{cm}^3/\text{g}$ )	Pore size (nm)
$\text{H}\beta$	-	492	0.48	3.90
$\text{Fe}_2\text{O}_3(8\%)/\text{H}\beta$	8.2	446	0.46	3.81
$\text{Fe}_2\text{O}_3(16\%)/\text{H}\beta$	16.0	425	0.43	3.75
$\text{Fe}_2\text{O}_3(20\%)/\text{H}\beta$	19.8	396	0.41	3.62
$\text{Fe}_2\text{O}_3(25\%)/\text{H}\beta$	25.3	352	0.31	3.36
spent $\text{Fe}_2\text{O}_3(20\%)/\text{H}\beta$	19.5	177	0.20	4.58

<sup>a</sup> Deduced from ICP analysis.

<sup>b</sup> Specific surface area calculated by the BET method.

<sup>c</sup> Total pore volume determined at  $P/P_0 = 0.99$ .

The  $\text{N}_2$  adsorption/desorption curves in Fig. 4 obtained from parent  $\text{H}\beta$  and  $\text{Fe}_2\text{O}_3(x)/\text{H}\beta$  samples showed the typical structure of mesoporosity, namely type-IV isotherms with well-defined hysteresis loops. A typical H4 type hysteresis loop was observed in the  $P/P_0$  range from 0.4 to 0.9, indicating the existence of large mesopores<sup>18, 19</sup>.

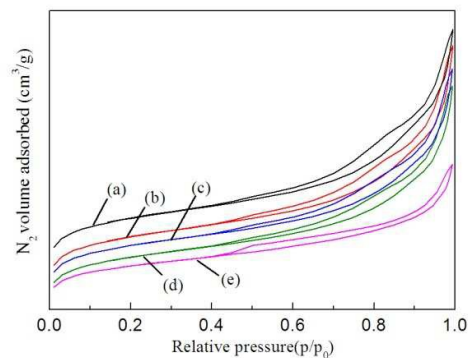


Fig. 4.  $\text{N}_2$  adsorption/desorption curves of  $\text{H}\beta$  and  $\text{Fe}_2\text{O}_3(x)/\text{H}\beta$   
(a) parent  $\text{H}\beta$ ; (b)  $\text{Fe}_2\text{O}_3(8\%)/\text{H}\beta$ ; (c)  $\text{Fe}_2\text{O}_3(16\%)/\text{H}\beta$ ; (d)  $\text{Fe}_2\text{O}_3(20\%)/\text{H}\beta$  and (e)  $\text{Fe}_2\text{O}_3(25\%)/\text{H}\beta$

The textural properties including BET surface area, pore volume, and pore size of parent  $\text{H}\beta$  and  $\text{Fe}_2\text{O}_3(x)/\text{H}\beta$  samples distributions were summarized in Table 1. Parent  $\text{H}\beta$  zeolite possessed the highest specific surface area ( $492 \text{ m}^2/\text{g}$ ), pore volume ( $0.48 \text{ cm}^3/\text{g}$ ) and pore size (3.90 nm). The increase of the  $\text{Fe}_2\text{O}_3$  loading from 8% to 25% led to a decrease in the specific surface area from  $446 \text{ m}^2/\text{g}$  to  $352 \text{ m}^2/\text{g}$ , the total pore volume from  $0.46 \text{ cm}^3/\text{g}$  to  $0.31 \text{ cm}^3/\text{g}$  and the pore size from 3.81 nm to 3.36 nm. The decrease of pore volume and pore size after loading  $\text{Fe}_2\text{O}_3$  is expected to improve the *para*-selectivity, since narrowed pores are benefit to shape-selective action. The severe decrease in specific surface area and

## ARTICLE

## Journal Name

total porous volume observed for the  $\text{Fe}_2\text{O}_3(25\%)/\text{H}\beta$  solid sample could be explained by blocking of pores due to the high loading of  $\text{Fe}_2\text{O}_3$ . The pore size decreased in the order: parent of  $\text{H}\beta > \text{Fe}_2\text{O}_3(8\%)/\text{H}\beta > \text{Fe}_2\text{O}_3(16\%)/\text{H}\beta > \text{Fe}_2\text{O}_3(20\%)/\text{H}\beta > \text{Fe}_2\text{O}_3(25\%)/\text{H}\beta$ .

The specific surface area and pore volume of the spent  $\text{Fe}_2\text{O}_3(20\%)/\text{H}\beta$  decreased remarkably to  $177 \text{ m}^2/\text{g}$  and  $0.20 \text{ cm}^3/\text{g}$ , which could be caused by carbonaceous deposits on the surface and inside the pores of the spent  $\text{Fe}_2\text{O}_3(20\%)/\text{H}\beta$  zeolite. The increase in pore size (4.58 nm) observed for the spent  $\text{Fe}_2\text{O}_3(20\%)/\text{H}\beta$  further confirmed blockage of micropores during the reaction by carbonaceous deposition.

**Acidity characterization**

The acid properties of zeolites are important in determining the catalytic activity and product selectivity for any catalyzed reaction. Acidic measurement was achieved by  $\text{NH}_3$ -TPD and Py-IR characterization.  $\text{NH}_3$ -TPD curves of parent  $\text{H}\beta$  and  $\text{Fe}_2\text{O}_3(x)/\text{H}\beta$  were showed in Fig.5.

Two peaks could be detected at  $240^\circ\text{C}$  and  $460^\circ\text{C}$  in the curve of parent  $\text{H}\beta$ , which were attributed to weak acid sites and strong acid sites, respectively. The number of weak acid sites was obviously greater than that of strong acid sites. Compared to parent  $\text{H}\beta$ , the desorption peak of weak acid sites in  $\text{Fe}_2\text{O}_3(x)/\text{H}\beta$  shifted slightly toward higher temperatures with the increase of  $\text{Fe}_2\text{O}_3$  loading. It indicated that the strength of weak acid increased slightly. The acid amount changed after the addition of  $\text{Fe}_2\text{O}_3$  too, the weak acid sites in  $\text{Fe}_2\text{O}_3(x)/\text{H}\beta$  decreased gradually with increasing of  $x$ , while strong acid sites of all the  $\text{Fe}_2\text{O}_3(x)/\text{H}\beta$  almost vanish. This result showed that  $\text{Fe}_2\text{O}_3$  preferentially acted with the strong acid sites of  $\text{H}\beta$  zeolite. In addition, the loading of  $\text{Fe}_2\text{O}_3$  is benefit to increase selectivity to PTBT by suppressing the further isomerization of formed PTBT to MTBT and this will be discussed later in section 3.3. The total acid amount decreased in the order of parent  $\text{H}\beta > \text{Fe}_2\text{O}_3(8\%)/\text{H}\beta > \text{Fe}_2\text{O}_3(16\%)/\text{H}\beta > \text{Fe}_2\text{O}_3(20\%)/\text{H}\beta > \text{Fe}_2\text{O}_3(25\%)/\text{H}\beta$ .

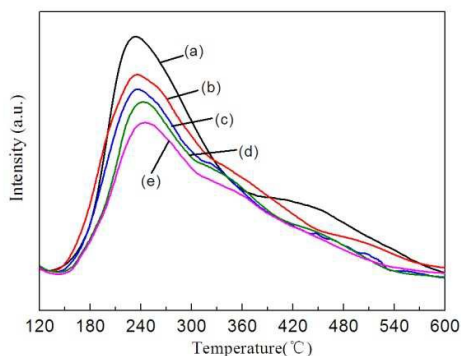


Fig.5.  $\text{NH}_3$ -TPD patterns of  $\text{H}\beta$  and  $\text{Fe}_2\text{O}_3(x)/\text{H}\beta$

(a) parent  $\text{H}\beta$ ; (b)  $\text{Fe}_2\text{O}_3(8\%)/\text{H}\beta$ ; (c)  $\text{Fe}_2\text{O}_3(16\%)/\text{H}\beta$ ; (d)  $\text{Fe}_2\text{O}_3(20\%)/\text{H}\beta$  and (e)  $\text{Fe}_2\text{O}_3(25\%)/\text{H}\beta$

Table 2 showed Py-IR spectra of parent  $\text{H}\beta$  and  $\text{Fe}_2\text{O}_3(x)/\text{H}\beta$ . It could be clearly seen from Table 2 that the total acid amount determined by Py-IR correlated well with the  $\text{NH}_3$ -TPD results and the relative amounts of B acid and L acid of  $\text{H}\beta$  changed significantly after loading  $\text{Fe}_2\text{O}_3$ . Upon increasing the  $\text{Fe}_2\text{O}_3$  content, both the B acid and L acid decreased. This is possibly because  $\text{Fe}_2\text{O}_3$  would cover some acid sites on  $\text{H}\beta$  zeolite. However, it's worth noting that

the B/L ratio first increased then dropped. It meant that L acid decreased more drastically than B acid. This may be attributed the electronic structure of transition metal elements. Most of the transition metal elements has empty orbit, which can be used as the "transferring station" for electron. This special electronic structure can make transition metal cation to interact with the framework via a polarizing or inductive effect, withdraw electrons from O-H bonds, thereby increase the B acidity<sup>20</sup>. As a result, the increased B acidity can compensate for the original B acidity covered by  $\text{Fe}_2\text{O}_3$ , to some degree. In addition, both B acid and L acid of  $\text{Fe}_2\text{O}_3(25\%)/\text{H}\beta$  were sharply reduced compared to those of  $\text{Fe}_2\text{O}_3(20\%)/\text{H}\beta$ , which can be attributed to blocking of pores of  $\text{H}\beta$  owing to the high  $\text{Fe}_2\text{O}_3$  loading in the former. As proposed above based on the  $\text{N}_2$  adsorption analysis, thus decreasing the total acid amount. The B acid amount decreased in the order of parent  $\text{H}\beta > \text{Fe}_2\text{O}_3(8\%)/\text{H}\beta > \text{Fe}_2\text{O}_3(16\%)/\text{H}\beta > \text{Fe}_2\text{O}_3(20\%)/\text{H}\beta > \text{Fe}_2\text{O}_3(25\%)/\text{H}\beta$ .

Table 2 Acidic properties of catalysts determined by Py-IR at  $150^\circ\text{C}$ .

Catalysts	B acid <sup>a</sup> ( $\mu\text{mol}/\text{g}$ )	L acid <sup>b</sup> ( $\mu\text{mol}/\text{g}$ )	Total acid ( $\mu\text{mol}/\text{g}$ )	B/L ratio
parent $\text{H}\beta$	84.2	47.2	131.4	1.78
$\text{Fe}_2\text{O}_3(8\%)/\text{H}\beta$	81.4	44.3	125.7	1.84
$\text{Fe}_2\text{O}_3(16\%)/\text{H}\beta$	78.9	41.2	120.1	1.92
$\text{Fe}_2\text{O}_3(20\%)/\text{H}\beta$	75.4	37.3	112.7	2.02
$\text{Fe}_2\text{O}_3(25\%)/\text{H}\beta$	63.2	32.5	95.7	1.94

<sup>a</sup> Deduced from the intensity of the band located at around  $1540 \text{ cm}^{-1}$ .

<sup>b</sup> Deduced from the intensity of the band located at around  $1450 \text{ cm}^{-1}$ .

**3.3 Catalytic activity evaluation**

Table 3 presented the results of toluene conversion and PTBT selectivity in the alkylation of toluene with TBA. Two monoalkylated products were detected. One was PTBT (para-isomer), which is in large amount, and the other was MTBT (meta-isomer). However, the OTBT (ortho-isomer) was not detected. The PTBT is desirable product since para-position is favored by the influence of the steric hindrance of methyl group and voluminous *tert*-butyl group on one hand, and by shape-selective action due to the regular channel structure of zeolite catalysts on the other hand. The formation of OTBT is hindered by ortho-position of methyl group and *tert*-butyl group. Trace amount of di-alkylated product 3,5-di-*tert*-butyltoluene (3,5-DTBT) from further alkylation of the monoalkylated products PTBT and MTBT was also detected. This can be explained by the same steric effects, where all alkyl groups are in the meta-position.

Table 3 Products selectivity and catalyst activity

Catalyst	Toluene conversion (%)	Distribution of products (%)			PTBT selectivity (%)	MTBT selectivity (%)
		PTBT	MTBT	other		
parent $\text{H}\beta$	58.4	39.3	16.7	2.4	67.3	28.6
$\text{Fe}_2\text{O}_3(8\%)/\text{H}\beta$	56.0	43.4	10.9	1.7	77.5	19.5
$\text{Fe}_2\text{O}_3(16\%)/\text{H}\beta$	55.5	44.2	10.2	1.1	79.6	18.4
$\text{Fe}_2\text{O}_3(20\%)/\text{H}\beta$	54.7	44.6	9.8	0.3	81.5	17.9
$\text{Fe}_2\text{O}_3(25\%)/\text{H}\beta$	46.3	37.8	8.3	0.2	81.6	17.9

Reaction conditions:  $n$  (TBA):  $n$ (toluene)-3:1, catalyst-1.0 g, temperature-190°C, time-4 h, cyclohexane-60 ml

Of the catalysts investigated, parent H $\beta$  exhibited toluene conversion of 58.4% at 190 °C after 4 h. The toluene conversion of all the Fe<sub>2</sub>O<sub>3</sub>( $x$ )/H $\beta$  catalysts were slightly lower than that of parent H $\beta$ . In addition, with increasing the Fe<sub>2</sub>O<sub>3</sub> loading the toluene conversion of Fe<sub>2</sub>O<sub>3</sub>( $x$ )/H $\beta$  catalyst was decreased. This result agrees with the trend of B acidity of Fe<sub>2</sub>O<sub>3</sub>( $x$ )/H $\beta$  catalyst (Table 2), which also decreased with increasing the Fe<sub>2</sub>O<sub>3</sub> loading. As is well known, the alkylation of toluene with alcohols catalyzed by zeolites is commonly considered to proceed via carbonium ion mechanisms<sup>21</sup> and the B acid sites are active sites<sup>22, 23</sup>. Therefore, Lower B acidity led to a lower catalytic activity. The toluene conversion of 54.7% was observed over Fe<sub>2</sub>O<sub>3</sub>(20%)/H $\beta$  catalyst. With further increases the Fe<sub>2</sub>O<sub>3</sub> content to 25%, a sharp decrease in toluene conversion was observed. This is probably due to sharp decrease in B acid sites amount, which caused by blockage of pores by excess Fe<sub>2</sub>O<sub>3</sub>. In addition, the severely decrease in pore size would lead to poor adsorption and diffusion of reactants and products, and this is another reason for the poor catalytic activity for Fe<sub>2</sub>O<sub>3</sub>(25%)/H $\beta$  catalyst.

The selectivity to PTBT over parent H $\beta$  is only 67.3%, which much lower than those found for Fe<sub>2</sub>O<sub>3</sub>( $x$ )/H $\beta$  (around 80.0%). As shown in Fig.6, the lower selectivity for PTBT over H $\beta$  can be explained in three ways. i) The low *para*-selectivity can be attributed to the pore size of H $\beta$  zeolite. The dimensions of 12-ring portals of parent H $\beta$  are 0.67×0.66 nm, while the kinetic sizes are 0.58nm for PTBT and 0.65nm for MTBT. Therefore, the shape-selective action has less effect on the product selectivity to PTBT over H $\beta$  zeolite. ii) The high strong acid amount of the H $\beta$  (Fig.4) is also responsible to the low *para*-selectivity. Because the MTBT is the most thermodynamically favored, the kinetically favored PTBT is gradually transformed to MTBT by isomerization on acid sites. And the isomerization reaction occurs easily on the strong acidic sites<sup>24, 25</sup>. iii) The high of acidity of external surface also promotes isomerization of the formed PTBT to MTBT. The isomerization of formed PTBT to MTBT runs more easily over the active sites on the external surface, where it is not sterically hindered as in the pores of zeolite. The above three reasons lead to the low PTBT selectivity over parent H $\beta$ .

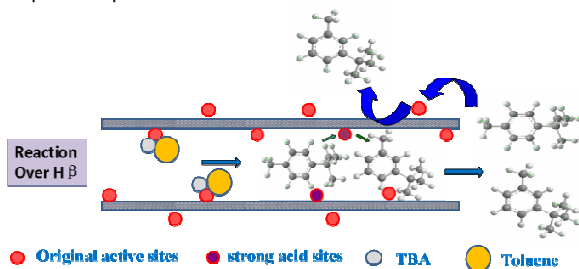


Fig.6 The mechanism for low PTBT selectivity over parent H $\beta$  zeolite

The PTBT selectivity over all the Fe<sub>2</sub>O<sub>3</sub>( $x$ )/H $\beta$  catalysts were around 80.0%, showing that upon loading of Fe<sub>2</sub>O<sub>3</sub>, the PTBT selectivity increased significantly. A possible mechanism was proposed to explain the effect of Fe<sub>2</sub>O<sub>3</sub> on the PTBT selectivity of

the catalyst, as sketched in Fig.7, and explains the increased selectivity in three ways. i) One reason because the narrowed pore size upon loading the Fe<sub>2</sub>O<sub>3</sub>. The pore size of Fe<sub>2</sub>O<sub>3</sub>( $x$ )/H $\beta$  catalyst was decreased with increasing the Fe<sub>2</sub>O<sub>3</sub> loading (Table 1). The narrowed pores of Fe<sub>2</sub>O<sub>3</sub>( $x$ )/H $\beta$  catalysts were benefit to formation of PTBT. Since the steric restriction with narrowed pores of Fe<sub>2</sub>O<sub>3</sub>( $x$ )/H $\beta$ , the PTBT with lower kinetic diameter (0.58 nm) can diffuse through the narrowed pores of Fe<sub>2</sub>O<sub>3</sub>( $x$ )/H $\beta$  more easily than MTBT with higher kinetic diameter (0.65 nm). ii) The decrease in strong acid sites could improve the *para*-selectivity. As discussed in section 3.2 (Fig.5), the weak acid sites in Fe<sub>2</sub>O<sub>3</sub>( $x$ )/H $\beta$  decreased gradually with increasing of  $x$ , while strong acid sites of all the Fe<sub>2</sub>O<sub>3</sub>( $x$ )/H $\beta$  almost vanish. Less strong acid sites caused by the loading of Fe<sub>2</sub>O<sub>3</sub> is benefit to increase selectivity to PTBT by suppressing the further isomerization of PTBT on acid sites. iii) In addition, the increase in PTBT selectivity could also be attributed to the deactivation of acid sites on surface of Fe<sub>2</sub>O<sub>3</sub>( $x$ )/H $\beta$  caused by the loading of Fe<sub>2</sub>O<sub>3</sub>. The isomerization of the formed PTBT to MTBT runs more easily over the active sites on the external surface, and less acid sites on surface reduce the isomerization reaction. As a result, loading Fe<sub>2</sub>O<sub>3</sub> on H $\beta$  catalysts could enhance and retain constant high *para*-selectivity.

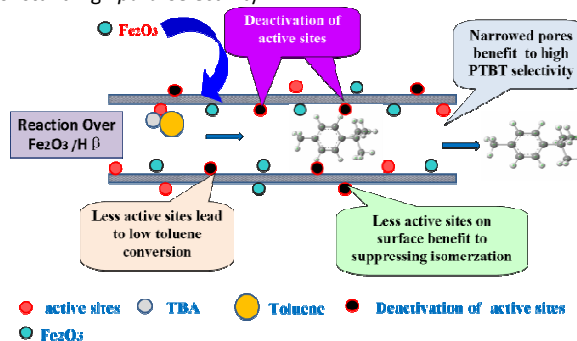


Fig.7 The mechanism for high PTBT selectivity over Fe<sub>2</sub>O<sub>3</sub>( $x$ )/H $\beta$  zeolite

## Conclusions

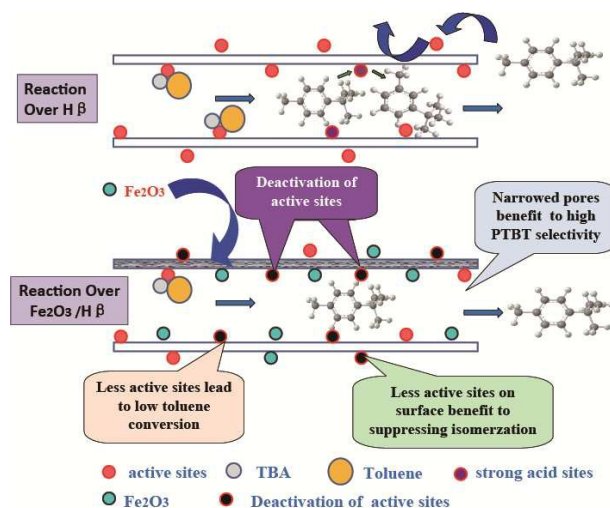
In the present work, Fe<sub>2</sub>O<sub>3</sub>( $x$ )/H $\beta$  catalysts with different Fe<sub>2</sub>O<sub>3</sub> loading were successfully prepared, and the effects of Fe<sub>2</sub>O<sub>3</sub> loading on the catalytic properties for alkylation toluene with TBA were studied. The acidity characterization results showed that modification of H $\beta$  with Fe<sub>2</sub>O<sub>3</sub> could increase the weak acid strength. However, the weak acid sites in Fe<sub>2</sub>O<sub>3</sub>( $x$ )/H $\beta$  decreased gradually with increasing of  $x$ , while strong acid sites of all the Fe<sub>2</sub>O<sub>3</sub>( $x$ )/H $\beta$  almost vanish. Both the B acid amount and total acid amount decreased in the order of parent H $\beta$  > Fe<sub>2</sub>O<sub>3</sub>(8%)/H $\beta$  > Fe<sub>2</sub>O<sub>3</sub>(16%)/H $\beta$  > Fe<sub>2</sub>O<sub>3</sub>(20%)/H $\beta$  > Fe<sub>2</sub>O<sub>3</sub>(25%)/H $\beta$ . The textural properties characterization results showed that parent H $\beta$  zeolite possessed the highest specific surface area (492 m<sup>2</sup>/g), pore volume (0.48 cm<sup>3</sup>/g) and pore size (3.90 nm). The increase of the Fe<sub>2</sub>O<sub>3</sub> loading from 8% to 25% led to a decrease in the pore size from 3.81 nm to 3.36 nm. The pore size decreased in the order of parent H $\beta$  > Fe<sub>2</sub>O<sub>3</sub>(8%)/H $\beta$  > Fe<sub>2</sub>O<sub>3</sub>(16%)/H $\beta$  > Fe<sub>2</sub>O<sub>3</sub>(20%)/H $\beta$  > Fe<sub>2</sub>O<sub>3</sub>(25%)/H $\beta$ .

The catalytic activity results showed that the toluene conversion over parent H $\beta$ , which possessed the largest B acidity (84.2 μmol/g),

exhibited the highest activity of 58.4% at 190 °C after 4 h. However, the PTBT selectivity over parent H $\beta$  was the lowest (67.3%). The dimensions of 12-ring portals of parent H $\beta$  are 0.67 nm  $\times$  0.66 nm, while the kinetic sizes are 0.58 nm for PTBT and 0.65 nm for MTBT. Therefore, the shape-selective action has less effect on the product selectivity to PTBT over H $\beta$  zeolite. In addition, further isomerization of formed PTBT to MTBT on acid sites also decreased the para-selectivity. The toluene conversion of 54.7% with PTBT selectivity of 81.5% was observed over Fe<sub>2</sub>O<sub>3</sub>(20%)/H $\beta$  catalyst at 190 °C after 4h. The selectivity to PTBT was improved significantly from 67.3% to 81.5%. A possible mechanism was proposed to explain the increased selectivity in three ways. i) The narrowed pores of Fe<sub>2</sub>O<sub>3</sub>(x)/H $\beta$  catalysts were benefit to formation of PTBT, since the PTBT with lower kinetic diameter (0.58 nm) can diffuse through the narrowed pores of Fe<sub>2</sub>O<sub>3</sub>(x)/H $\beta$  more easily than MTBT with higher kinetic diameter (0.65 nm) because of its steric restriction with narrowed pores of Fe<sub>2</sub>O<sub>3</sub>(x)/H $\beta$ . ii) The deactivation of acid sites caused by the loading of Fe<sub>2</sub>O<sub>3</sub> is benefit to increase selectivity to PTBT by suppressing the further isomerization of PTBT on acid sites. As a result, the Fe<sub>2</sub>O<sub>3</sub>(x)/H $\beta$  catalysts could enhance and retain constant high para-selectivity. However, a significant deactivation of catalysts containing 25% of Fe<sub>2</sub>O<sub>3</sub> was observed and attributed to a pore blocking phenomenon by excess Fe<sub>2</sub>O<sub>3</sub>. With further increases the Fe<sub>2</sub>O<sub>3</sub> content to 25%, a sharp decrease in toluene conversion was observed, which is mainly due to sharp decrease in B acid sites amount, which caused by blockage of pores by excess Fe<sub>2</sub>O<sub>3</sub>.

## References

1. Y. Sun and R. Prins, *Appl. Catal. A-Gen*, 2008, 336, 11-16.
2. C. Sievers, J. S. Liebert, M. M. Stratmann, R. Olindo and J. A. Lercher, *Appl. Catal. A-Gen*, 2008, 336, 89-100.
3. H. Nur, Z. Ramli, J. Efendi, A. N. A. Rahman, S. Chandren and L. S. Yuan, *Catal. Commun.*, 2011, 12, 822-825.
4. W. Y. Li, Y. H. Xu, J. Q. Wang, Z. B. Zhai, Z. Y. Yan and Y. L. Yang, *Catal. Lett.*, 2007, 119, 327-331.
5. W. Y. Zhou, J. G. Pan, F. A. Sun, K. Huang, M. Y. He and Q. Chen, *React. Kinet. Mech. Cat.*, 2016, 117, 789-799.
6. W. H. Yu, Z. R. Zhang, H. Wang, Z. H. Ge. and T. J. Pinnavaia, *Micropor. Mesopor. Mater.*, 2007, 104, 151-158.
7. S. Pai, U. Gupta and S. Chilukuri, *J. Mol. Catal. A- Chem.*, 2007, 265, 109-116.
8. D. Mravec, P. Zavadan and A. Kaszonyi, *Appl. Catal. A-Gen.*, 2004, 257, 49-55.
9. Y. Y. Wang, H. Song, H. L. Song, X. L. Sun and X. Q. Wang, *Prog. React. Kinet. and Mec.*, 2016, 41, 126-134.
10. H. K. Min, S. H. Cha and S. B. Hong, *Acs Catal.*, 2012, 2, 971-981.
11. J. C. Jansen, E. J. Creighton, S. L. Njo, H. V. Koningsveld and H. V. Bekkum, *Catal. Today*, 1997, 38, 205-212.
12. K. F. Liu, S. J. Xie, S. L. Liu, G. L. Xu, N. N. Gao and L. Y. Xu, *J. Catal.*, 2011, 283, 68-74.
13. B. Xue, Y. X. Li and L. J. Deng, *Catal. Commun.*, 2009, 10, 1609-1614.
14. T. Nobukawa, M. Yoshida, Satoshi Kameoka, S. Ito, A. Keiichi Tomishige and K. Kunimori, *J. Phys. Chem. B*, 2004, 108, 4071-4079.
15. M. Mauvezin, G. Delahay, B. Coq, S. Kieger, a. J. C. Jumas and J. OlivierFourcade, *J. Phys. Chem. B*, 2001, 105, 928-935.
16. C. H. He, Y. H. Wang, Y. S. Cheng, C. K. Lambert and R. T. Yang, *Appl. Catal. A-Gen.*, 2009, 368, 121-126.
17. F. Richard, S. Célérier, M. Vilette, J. D. Comparot and V. Montouillout, *Appl. Catal. B-Environ.*, 2014, s 152-153, 241-249.
18. S. S. Vieira, Z. M. Magriotis, M. F. Ribeiro, I. Graça, A. Fernandes, J. M. F. M. Lopes, S. M. Coelho, N. A. V. Santos and A. A. Saczk, *Micropor. Mesopor. Mater.*, 2015, 201, 160-168.
19. N. Kasian, E. Verheyen, G. Vanbutsele, K. Houthoofd, T. I. Koranyi, J. A. Martens and C. E. A. Kirschhock, *Micropor. Mesopor. Mater.*, 2013, 166, 153-160.
20. R. Carvajal, P. J. Chu and J. H. Lunsford, *J. Catal.*, 1990, 125, 123-131.
21. M. Selvaraj, S. H. Jeon, J. Han, P. K. Sinha and T. G. Lee, *Appl. Catal. A-Gen.*, 2005, 286, 44-51.
22. M. T. Portilla, F. J. Llopis and C. Martínez, *Appl. Catal. A - Gen.*, 2011, 393, 257-268.
23. L. Chen, H. Dong and L. Shi, *Ind. Eng. Chem. Res.*, 2010, 49, 7234-7238.
24. I. Fechete, P. Caullet, E. Dumitriu, V. Hulea and H. Kessler, *Appl. Catal. A-Gen.*, 2005, 280, 245-254.
25. E. Dumitriu, D. Meloni, R. Monaci and V. Solinas, *CR.chim*, 2005, 8, 441-456.



TOC: The alkylation of toluene with *tert*-butyl alcohol to produce 4-*tert*-butyltoluene over Fe<sub>2</sub>O<sub>3</sub>(x)/H $\beta$  was discussed. Modification by Fe<sub>2</sub>O<sub>3</sub> is a highly efficient method for improving the *para*-selectivity by adjusting pore entrance and reducing the strong acid sites and external acid sites.